Radiology

ORIGINAL RESEARCH • GASTROINTESTINAL IMAGING

Liver Fat Content Measurement with Quantitative CT Validated against MRI Proton Density Fat Fraction: A Prospective Study of 400 Healthy Volunteers

Zhe Guo, MD • Glen M. Blake, PhD • Kai Li, MD • Wei Liang, BS • Wei Zhang, BS • Yong Zhang, MD • Li Xu, MD • Ling Wang, MD • J. Keenan Brown, PhD • Xiaoguang Cheng, MD • Perry J. Pickhardt, MD

From the Department of Radiology, Beijing Jishuitan Hospital, 31 Xinjiekou East Street, Beijing 100035, China (Z.G., K.L., W.L., W.Z., Y.Z., L.X., L.W., X.C.); School of Biomedical Engineering & Imaging Sciences, King's College London, St Thomas' Hospital, London, England (G.M.B.); Mindways Software Inc, Austin, Tex (J.K.B.); and Department of Radiology, University of Wisconsin School of Medicine and Public Health, Madison, Wis (P.J.P.). Received February 28, 2019; revision requested May 7; revision received September 5; accepted September 13. **Address correspondence to** X.C. (e-mail: *Xiao65@263.net*).

Conflicts of interest are listed at the end of this article.

Radiology 2019; 00:1–9 • https://doi.org/10.1148/radiol.2019190467 • Content code: GI

Background: Although chemical shift–encoded (CSE) MRI proton density fat fraction (PDFF) is the current noninvasive reference standard for liver fat quantification, the liver is more frequently imaged with CT.

Purpose: To validate quantitative CT measurements of liver fat against the MRI PDFF reference standard.

Materials and Methods: In this prospective study, 400 healthy participants were recruited between August 2015 and July 2016. Each participant underwent same-day abdominal unenhanced quantitative CT with a calibration phantom and CSE 3.0-T MRI. CSE MRI liver fat measurements were used to calibrate an equation to adjust CT fat measurements and put them on the PDFF measurement scale. CT and PDFF liver fat measurements were plotted as histograms, medians, and interquartile ranges compared; scatterplots and Bland-Altman plots obtained; and Pearson correlation coefficients calculated. Receiver operating characteristic curves including areas under the curve were evaluated for mild (PDFF, 5%) and moderate (PDFF, 14%) steatosis thresholds for both raw and adjusted CT measurements. Sensitivity, specificity, positive predictive value, and negative predictive value were calculated.

Results: Four hundred volunteers (mean age, 52.6 years ± 15.2; 227 women) were evaluated. MRI PDFF measurements of liver fat ranged between 0% and 28%, with 41.5% (166 of 400) of participants with PDFF greater than 5%. Both raw and adjusted quantitative CT values correlated well with MRI PDFF (r^2 = 0.79; $P < .001$). Bland-Altman analysis of adjusted CT values showed no slope or bias. Both raw and adjusted CT had areas under the receiver operating characteristic curve of 0.87 and 0.99, respectively, to identify participants with mild (PDFF, >5%) and moderate (PDFF, >14%) steatosis, respectively. The sensitivity, specificity, positive predictive value, and negative predictive value for unadjusted CT was 75.9% (126 of 166), 85.0% (199 of 234), 78.3% (126 of 161), and 83.3% (199 of 239), respectively, for PDFF greater than 5%; and 84.8% (28 of 33), 98.4% (361 of 367), 82.4% (28 of 34), and 98.6% (361 of 366), respectively, for PDFF greater than 14%. Results for adjusted CT were mostly identical.

Conclusion: Quantitative CT liver fat exhibited good correlation and accuracy with proton density fat fraction measured with chemical shift–encoded MRI.

Online supplemental material is available for this article.

Nonalcoholic fatty liver disease has a global prevalence of 25% and is defined as the intracellular accumulation of fat in the liver parenchyma exceeding 5% in the absence of competing causes such as chronic viral hepatitis, drug-induced steatosis, or other chronic liver diseases such as autoimmune hepatitis, hemochromatosis, or alcohol abuse (1,2). Nonalcoholic fatty liver disease is considered an important cause of chronic liver disease, such as nonalcoholic steatohepatitis and cirrhosis, and even hepatocellular carcinoma (3). People with nonalcoholic fatty liver disease tend to also have obesity, diabetes, dyslipidemia, and hypertension, and are at higher risk of cardiovascular disease (1). Accurate and reliable quantification of liver fat content is critical for the diagnosis, treatment, and monitoring of nonalcoholic fatty liver disease.

Liver biopsy has long been the reference standard for assessment of liver fat content, although its application is restricted because of its invasive nature and high cost (4). Noninvasive techniques include US, CT, and MRI. US is an inexpensive and convenient diagnostic tool for nonalcoholic fatty liver disease, but it is semiquantitative and relatively insensitive to individuals with liver fat content less than 20% (5–7). Traditionally, CT was considered accurate for moderate-to-severe steatosis but insensitive to mild steatosis (8,9), and the results are susceptible to variable scanning conditions such as different tube voltages and CT scanners from different manufacturers (9,10). MRI methods, including proton MR spectroscopy and the emerging technique of chemical shift–encoded (CSE) MRI, are regarded as the most accurate noninvasive techniques for the evaluation of liver fat (11–15). Proton MR spectroscopy and CSE MRI quantify liver fat directly in terms of the proton density fat fraction (PDFF), defined as the ratio of the signal strength from fat to the total signal from fat and water (11,16).

Abbreviations

CSE = chemical shift encoded, PDFF = proton density fat fraction, ROI = region of interest

Summary

Liver fat measurement at quantitative CT in adults aged 22–83 years agreed well with MRI liver proton density fat fraction and could serve as a useful tool for assessing hepatic steatosis.

Key Results

- Quantitative CT measurements for liver fat correlated well with MRI liver proton density fat fraction (PDFF; $r^2 = 0.79$; $P < .001$), without a slope or bias at Bland-Altman analysis.
- Areas under the receiver operating characteristic curve were 0.87 and 0.99 for quantitative CT to identify healthy volunteers with mild (PDFF, >5%) and moderate (PDFF, >14%) steatosis, respectively.
- Quantitative CT could allow for noninvasive and quantitative detection of hepatic steatosis.

Quantitative CT was initially developed for the measurement of bone mineral density (17). Use of calibration materials with a large variation in the relative contributions of photoelectric and Compton scattering to measured phantom x-ray attenuation enables the evaluation of soft tissue composition in nonosseous tissues such as the liver. Unlike traditional semiquantitative CT approaches, quantitative CT has the potential to help directly measure liver fat content and the calibration phantom makes it possible to undertake multicenter studies by using CT scanners from different manufacturers. We previously described (18) a method of abdominal quantitative CT scans to help quantify liver fat content and we validated it at dual-energy CT. In a subsequent study, Xu et al (19) used goose liver samples to validate the measurement of liver fat content with quantitative CT by comparing it with CSE MRI PDFF and biochemical extraction.

The purpose of our study was to validate the accuracy of quantitative CT in the measurement of liver fat by using CSE MRI PDFF as reference standard in a large prospective human cohort.

Materials and Methods

This prospective study was approved by the ethics committee of our institution and participants provided written informed consent. The study was supported by the Beijing Bureau of Health 215 program (grant number 2009–2-03). J.K.B. is an employee of Mindways Software (Austin, Tex). He had no control of inclusion of data or information submitted for publication. Other authors had no relevant conflicts of interest.

Study Participants

Four hundred healthy adults and older adults (age, >65 years) without serious health problems were recruited from communities near the Beijing Jishuitan Hospital (Beijing, China). The age of the volunteers was widely distributed between 22 and 83 years. Inclusion criteria were healthy people able to give informed consent. Exclusion criteria were pregnant women, individuals with metal implants in the thoracolumbar spine; a history of hepatic lobectomy, cirrhosis, or hemochromatosis; or people who were intolerant of MRI examination because of claustrophobia.

Quantitative CT Scan Protocol and Measurement of Liver Fat

We performed quantitative CT by using a scanner (Aquilion Prime ESX-302A; Toshiba Medical Systems, Otawara, Japan) with a five-rod calibration phantom (Model 3 phantom; Mindways Software) with an aqueous K_2HPO_4 bone density standard placed beneath the participants. The scan range included the whole liver and spleen. Scan parameters were 120 kVp; 187 mAs; pitch, 0.637; rotation time, 0.75 second; collimation, 40 cm; table height, 120 cm; field of view, 500 mm; and thickness, 1 mm. Reconstruction parameters were standard algorithm, 1-mm section thickness and interval, and 400-mm display field of view.

We measured liver fat by using an application (QCT Pro 6.0 Supplementary Tissue Measurements; Mindways Software). This application measures liver fat content directly in regions of interest (ROIs) drawn on the liver parenchyma on the basis of Hounsfield units and data from the calibration phantom. ROIs were placed on the section at which the right branch of the portal vein enters the liver. Three ROIs, each with an area of 300 mm^2 (deviation < 10 mm^2), were placed in the peripheral area of the left lobe, the right anterior lobe, and the right posterior lobe (Fig 1a). If the left lobe was not visible at this level, the section at which the left lobe had the largest transverse area was chosen for the measurement. The ROIs were selected to avoid the major blood vessels and bile ducts, intrahepatic calcification, liver cysts, artifacts caused by the ribs, and gas in the lung or gastrointestinal tract. The

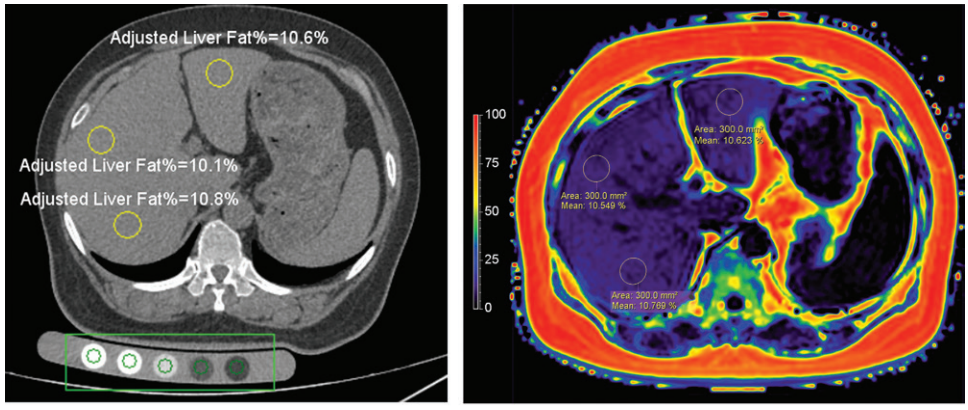

a. b.

Figure 1: Liver fat content measurement with **(a)** quantitative CT and **(b)** chemical shift–encoded MRI in a 57-year-old woman. Three regions of interest (ROIs) were placed in the peripheral areas of the left lobe, right anterior lobe, and right posterior lobe of the liver, and the average of the three ROIs was chosen for the liver fat content.

average of the three ROIs was used for the final quantitative CT measurement of liver fat.

CSE MRI Protocol and MRI Measurement of Liver Fat

On the same day as the quantitative CT examination, the participants underwent a multiecho three-dimensional spoiled gradient-echo sequence, referred to as an mDixon Quant study, by using a 3.0-T MRI system with a 32-channel torso body coil (Ingenia, Philips Healthcare, Best, the Netherlands). The mDixon Quant sequence is used to generate water, fat, T2*, and R2* images, with in-phase and opposed-phase images that were synthesized from the water-fat images. The imaging parameters were as follows: repetition time msec/echo time msec, 6.2/0.95; six echoes with echo time shift, 0.8 msec; field of view, 360 × 330 × 120 mm^3; flip angle, 3°; voxel size, 2.5 × 2.5 × 3.0 mm^3; sensitivity encoding, two; two signal averages; and imaging time, 12.5 msec.

The CSE MRI data were processed with software (ISP version 7; Philips Healthcare, Best, the Netherlands). Confounder-corrected PDFF maps were generated for measurements of PDFF. The sizes and locations of the three ROIs were manually matched with the quantitative CT images as closely as possible (Fig 1b). The average of three ROIs was again used for the MRI measurement of liver fat. R2* values in the same ROIs were also measured from R2* maps.

Quantitative CT and MRI Analysis

Two radiologists (Z.G., with 8 years of experience, and K.L., with 3 years of experience) analyzed the quantitative CT and MRI data, respectively, and were blinded to each other's findings. Repeated measurements were made in a randomly selected group of 30 participants to determine the intraobserver and interobserver precision of the MRI and CT results.

Comparison with Alternative CT Approaches to Liver Fat Quantification

Hounsfield units of the three ROIs in the liver consistent with quantitative CT and MRI measurements and a fourth ROI with the same area placed on the spleen were measured on the raw CT images (Radiant DICOM Viewer software version 4.6.9; Medixant, Poznan, Poland). The average of the three ROIs in the liver was used as the mean liver Hounsfield unit. The difference between liver and spleen Hounsfield units (ie, the liver-spleen Hounsfield unit difference) and the liver-to-spleen Hounsfield unit ratio were also recorded.

Statistical Analysis

Quantitative CT measurements of liver fat differed systematically from CSE MRI PDFF measurements for two reasons. First, although both responded to the fat content of tissue, they differed in the way that they responded to the fat-free content. Whereas MRI helps to measure the fat-free component in terms of the water signal (11), quantitative CT helps to measure it in terms of the x-ray attenuation of fat-free tissue, including both the water and nonaqueous components. In particular, the nonaqueous contents of lean tissue including protein and minerals contribute significantly to the x-ray attenuation coefficient of fat-free tissue measured in Hounsfield units, but they contribute little or nothing to the CSE MRI signal. Because water makes up only a certain fraction of the lean tissue mass measured at quantitative CT, when considered as a fraction of the total liver mass, MRI measurements of percentage fat content are systematically larger than quantitative CT measurements. Second, quantitative CT and MRI measurements may differ because of errors in determining the zero-point of the CT calibration scale. We therefore used the CT and MRI data to adjust the quantitative CT measurements to make them consistent with PDFF and ensure that the two measurements are directly comparable on the same scale over the range of 0%–100% liver fat.

A full description of how this adjustment is provided is in Appendix E1 (online). Briefly, by analogy with the definition of PDFF we define unadjusted quantitative CT measurements of liver fat by the following equation (18):

$$CTFF = \left(\frac{HU_{lean} - HU_{liver}}{HU_{lean} - HU_{fat}} \right) \quad (1),$$

where $CTFF$ is CT fat fraction, HU_{liver} is the measurement in Hounsfield units in the liver ROI, HU_{lean} is the value in Hounsfield units for fat-free liver tissue, and HU_{fat} is the value for 100% fat. Because HU_{liver} varies between HU_{lean} and HU_{fat}, the value of CT fat fraction varies from 0% to 100%. Values of HU_{lean} and HU_{fat} were determined from data from the calibration phantom and the composition of fat-free liver tissue and 100% fat by using a previously described method (18). We note that, because Hounsfield units are used to measure the linear x-ray attenuation coefficient, CT fat fraction represents the volume fraction of fat. The first step to adjust raw quantitative CT measurements and put them on the same measurement scale as PDFF is to apply a correction that allows for any error in the zero-point of the CT fat fraction measurement scale compared with the CSE MRI PDFF measurement scale by using the equation:

$$CTFF' = CTFF + Offset \quad (2),$$

where $CTFF$ is CT fat fraction defined by Equation (1), *offset* is a constant term that corrects for any error in the zero-point of the CT fat fraction scale, and $CTFF'$ is the corrected CT fat fraction. The second step is to convert CT fat fraction ($CTFF'$) defined by Equation (2) into equivalent values of PDFF by using the equation:

$$\text{Adjusted quantitative CT liver fat} = \left(\frac{CTFF'}{CTFF' + \alpha(1 - CTFF')} \right) \quad (3).$$

The derivation of Equation (3) is provided in Appendix E1 (online), which also explains how the PDFF and raw quantitative CT liver fat data for the 400 volunteers were used to derive

Table 1: Demographic Data

Parameter	Healthy (PDFF, <5%)	Mild Steatosis (PDFF, 5%–14%)	Moderate Steatosis (PDFF, >14%)	*P* Value, Mild Steatosis vs Healthy	*P* Value, Moderate Steatosis vs Healthy
No. of participants	234	133	33	.02	.02
Men	87	66	20		
Women	147	67	13		
Mean age (y)	51.4 ± 16.3 (22−83)	54.1 ± 13.4 (24−79)	54.5 ± 14.2 (29−79)	.10	.26
Mean body weight (kg)	64.5 ± 10.3 (45−100)	72.8 ± 13.1 (43.9−119)	78.7 ± 15.0 (51−120)	<.001	<.001
Mean height (cm)	162.6 ± 8.3 (140−187)	164.7 ± 8.4 (144−187)	164.4 ± 10.8 (140−184)	.03	.37
Mean BMI (kg/m^2)	24.4 ± 3.2 (16.1−34.9)	26.8 ± 3.8 (18.8−38.3)	28.9 ± 3.5 (21.2−35.4)	<.001	<.001

Note.—Mean data are ± standard deviation; data in parentheses are range. There was a total of 400 study participants. Participants were of Chinese Han ethnicity. BMI = body mass index, PDFF = proton density fat fraction.

the best-fit values of the offset and the coefficient α. To avoid bias the data for the 400 participants were divided into four validation sets each with 100 volunteers. For each validation set, the remaining 300 volunteers were used as a training set to derive values of the coefficient α and the offset. Equations (2) and (3) were then used with the values of α and the offset for each validation set to derive an adjusted CT liver fat result for every participant.

Continuous variables were expressed as means ± standard deviation. Categorical variables were expressed as numbers and percentages. The measurements of the intraobserver and interobserver precision were expressed as the root mean square standard deviation of the repeat measurements in units of percentage liver fat. PDFF and the unadjusted CT fat fraction liver fat measurements were plotted as histograms and the mean, standard deviation, median, and interquartile range were calculated. Scatterplots and Bland-Altman plots (20) were drawn to examine the relationships between unadjusted CT, adjusted CT, and PDFF results. On the basis of their PDFF results, participants were categorized as healthy (PDFF, <5%), mild (PDFF, 5%–14%), moderate (PDFF, 14%–28%), or severe (PDFF, >28%) steatosis (21). Receiver operating characteristic curves were established to determine the diagnostic accuracy of both unadjusted and adjusted CT with PDFF as reference standard, and the area under the receiver operating characteristic curve was calculated. Values of sensitivity, specificity, positive predictive value, and negative predictive value were calculated together with their corresponding Cohen κ indexes (22). The correlation between CSE MRI PDFF and unadjusted quantitative CT results was compared with three alternative CT approaches: PDFF values estimated from mean liver Hounsfield units by using a published calibration curve (23), liver-spleen Hounsfield unit difference, and liver-to-spleen Hounsfield unit ratio. A statistical website (*www.vassarstats.net*) was used for statistical computation. A *P* value less than .05 was considered to indicate statistical significance.

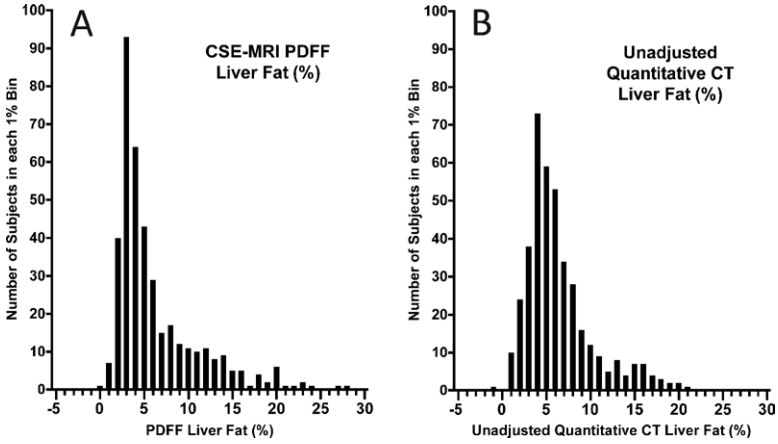

Figure 2: Histograms show measurements of, *A*, chemical shift–encoded (CSE) MRI proton density fat fraction (PDFF) and, *B*, unadjusted quantitative CT liver fat plotted as histograms in 1% bins.

Results

Demographic Data

Demographic data from the 400 volunteers (mean age, 52.6 years; age range, 22–83 years; 227 women) who participated in the study are in Table 1. The volunteers were of Chinese Han ethnicity. None of the volunteers were excluded from the statistical analysis. Normal liver fat content was found in 234 participants (58.5%), whereas 133 participants (33.3%), 32 participants (8.0%), and one participant (0.3%) had mild, moderate, or severe steatosis, respectively. A greater proportion of men had mild (*P* = .02) or moderate or severe steatosis (*P* = .02) compared with women. Study participants with higher PDFF also weighed more (*P* < .001) and had larger body mass index (*P* < .001). When men and women were considered separately, study participants of both sexes with higher PDFF were statistically significantly heavier and had a larger body mass index. MRI measurements of R2* ranged from 27 sec^{-1} to 104 sec^{-1} (mean, 51 sec^{-1}). When interpreted in terms of liver iron content, all results were within the normal range, and the errors in the CT measurements of liver fat because of liver iron content were all less than 1%.

Table 2: Comparison of Quantitative CT and Chemical Shift–encoded MRI Liver Fat Measurements

Statistic	CSE MRI PDFF Liver Fat (%)	Unadjusted Quantitative CT Liver Fat (%)	Adjusted Quantitative CT Liver Fat (%)	PDFF vs Unadjusted Quantitative CT	PDFF vs Adjusted Quantitative CT
Mean	6.30	6.39	6.30	.40	.99
Standard deviation	4.83	3.87	4.83	<.001	.50
Median	4.32	5.38	5.08	.002	.49
25th percentile	3.15	3.87	3.13	<.001	.95
75th percentile	8.22	7.67	7.95	.42	.18
Maximum value	28.23	21.22	24.38	…	…
Minimum value	0.10	−0.89	−3.09	…	…
Liver fat greater than 5%	41.5 (166/400)	57.2 (229/400)	50.8 (203/400)	<.001	.01
Liver fat greater than 14%	8.2 (33/400)	6.8 (27/400)	9.2 (37/400)	.50	.71

Note.—Liver fat greater than 5% refers to the percentage of participants with liver fat measurement greater than 5%; liver fat greater than 14% refers to the percentage of participants with liver fat measurement greater than 14%. Unadjusted quantitative CT refers to raw quantitative CT liver fat measurement reported by an application (QCT PRO 6.0 Supplementary Tissue Measurements, Mindways Software); adjusted quantitative CT refers to quantitative CT liver fat measurement corrected for zero-point calibration error and nonaqueous fat-free liver tissue. CSE = chemical shift encoded, PDFF = proton density fat fraction.

Distribution of MRI and Quantitative CT Liver Fat Measurements

Figure 2, *A*, *B*, shows the distributions of the measurements of CSE MRI PDFF and unadjusted CT liver fat, respectively, plotted as histograms. The CT measurements ranged from −0.9% to 21.2%, compared with 0.1%–28.2% for the PDFF measurements. Median values were 5.4% (interquartile range, 3.9%–7.7%) for CT compared with 4.3% (interquartile range, 3.2%–8.2%) for PDFF (Table 2). Values of intraobserver root-mean-square standard deviation for MRI and CT were 0.58% and 0.34%, respectively, and for interobserver root-mean-square standard deviation the values were 0.33% and 0.35%, respectively.

Correlation and Bland-Altman Analysis

Figure 3, *A*, *B*, shows the scatterplot and Bland-Altman plot, respectively, of CSE MRI PDFF against unadjusted CT liver fat. The scatterplot has a positive correlation (r^2 = 0.79; $P < .001$) and the Bland-Altman plot shows an excess of participants whose quantitative CT measurement exceeded their PDFF when average liver fat on the horizontal axis was less than 5% (142 of 217; $P < .001$), but the opposite bias for liver fat greater than 10% (12 of 66; $P < .001$). The Bland-Altman plot shows a negative correlation (r^2 = 0.19; $P < .001$) with an overall bias of 0.09% that was not different from 0 (P = .40).

Appendix E1 (online) discusses how PDFF and quantitative CT liver fat measurements for the 400 study participants were used to derive best-fit values for the calibration offset and the coefficient α (Eqq [2, 3]). The results for the offset for the four training sets were −1.45%, −1.42%, −1.52%, and −1.42%. The results for the coefficient α were .766, .756, .761, and .781 respectively. Figure 3, *C*, *D*, shows the scatterplot and Bland-Altman plot when CSE MRI PDFF was plotted against adjusted CT liver fat values for the validation data set. The adjusted CT measurements ranged from −3.1% to 24.4% (median, 5.1%; interquartile range, 3.1%–8.0%) (Table 2). The scatterplot has a positive correlation (r^2 = 0.79; $P < .001$), and the Bland-Altman plot no longer has an excess of participants with a positive bias among participants with liver fat values less than 5% (107 of 224; P = .55) or an excess with negative bias among participants with liver fat greater than 10% (35 of 69; $P > .99$). In Figure 3, *D*, the absolute value of the bias of the Bland-Altman plot was less than 0.01% and correlation coefficient was negligible ($r^2 <$ 0.001; P = .97).

Receiver Operating Characteristic Curves and Diagnostic Accuracy

Figure 4, *A*, *B*, shows the receiver operating characteristic curves for unadjusted CT liver fat to correctly classify participants with PDFF greater than 5% (mild steatosis threshold; area under the receiver operating characteristic curve, 0.87) and greater than 14% (moderate steatosis threshold; area under the receiver operating characteristic curve, 0.99), respectively. For the 5% threshold, sensitivity was 75.9% (126 of 166), specificity was 85.0% (199 of 234), positive predictive value was 78.3% (126 of 161), and negative predictive value was 83.3% (199 of 239). The corresponding values of Cohen κ were 59.7%, 62.8%, 62.8%, and 59.7%, respectively. For the 14% threshold, sensitivity was 84.8% (28 of 33), specificity was 98.4% (361 of 367), positive predictive value was 82.4% (28 of 34), and negative predictive value was 98.6% (361 of 366). The corresponding values of Cohen κ were 83.4%, 80.8%, 80.8%, and 83.4%, respectively.

Figure 4, *C*, *D*, shows the corresponding receiver operating characteristic curves for adjusted CT liver fat to correctly classify participants with PDFF greater than 5% (area under the receiver operating characteristic curve, 0.87) and greater than 14% (area under the receiver operating characteristic curve, 0.99). For the 5% threshold, the sensitivity, specificity, positive predictive value, and negative predictive value and their Cohen κ values were identical to those for unadjusted CT liver fat. For the 14% threshold, the sensitivity

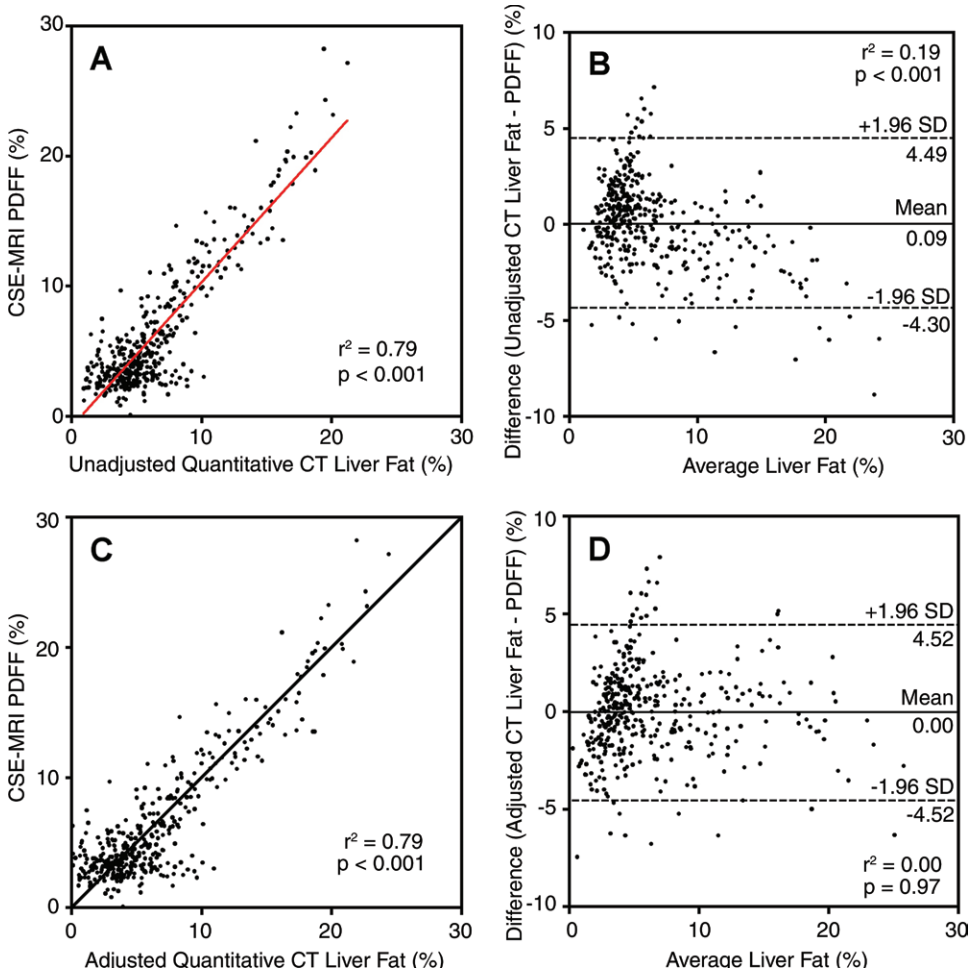

Figure 3: Plots show, *A*, scatterplot of chemical shift–encoded (CSE) MRI proton density fat fraction (PDFF) against the unadjusted quantitative CT liver fat, *B*, data points in *A* shown as a Bland-Altman plot, *C*, scatterplot of the CSE MRI PDFF against the adjusted quantitative CT liver fat, and, *D*, the data points in *C* shown as a Bland-Altman plot. SD = standard deviation.

was 84.8% (28 of 33), specificity was 98.6% (362 of 367), positive predictive value was 84.8% (28 of 33), and negative predictive value was 98.6% (362 of 367). The Cohen κ was 83.5% for all four measures.

Comparison with Alternative CT Approaches to Liver Fat Quantification

Figure 5 shows CSE MRI PDFF plotted against unadjusted quantitative CT, the PDFF value estimated from the mean liver Hounsfield units, liver-spleen Hounsfield unit difference, and liver-to-spleen Hounsfield unit ratio. When the data for PDFF estimated from Hounsfield units were plotted in the form of a Bland-Altman plot, the bias was −3.8% (not shown). When CSE MRI PDFF was plotted against the liver-spleen Hounsfield unit difference (Fig 5, *C*) and liver-to-spleen Hounsfield unit ratio (Fig 5, *D*) the correlation coefficients were significantly poorer (P = .03 and .002, respectively).

Discussion

Nonalcoholic fatty liver disease has become a global health problem and increased the economic burden on society, especially in developed countries (24,25). Accurate assessment of liver fat content is an essential prerequisite for treatment and follow-up of nonalcoholic fatty liver disease. MRI techniques, especially chemical shift–encoded (CSE) MRI, have become the noninvasive reference standard for the quantification of hepatic steatosis. Quantitative CT applied with unenhanced CT data is widely used for measuring bone mineral density and has proven potential for liver fat measurement in previous studies (18,19). Our study showed good agreement between the adjusted quantitative CT results and MRI proton density fat fraction (PDFF) as demonstrated by scatterplots and Bland-Altman plots, with close agreement between the means, medians, 25th and 75th percentiles, high areas under the receiver operating characteristic curve at 5% and 14% PDFF, and good sensitivity and specificity for diagnosing mild and moderate hepatic steatosis.

The different principles behind quantitative CT and CSE MRI lead to differences in the measurements of liver fat that have not been previously discussed. Our analysis of these differences (Appendix E1 [online]) led to a correction that enabled raw quantitative CT liver fat measurements to be adjusted and put on a scale consistent with MRI-derived PDFF measurements.

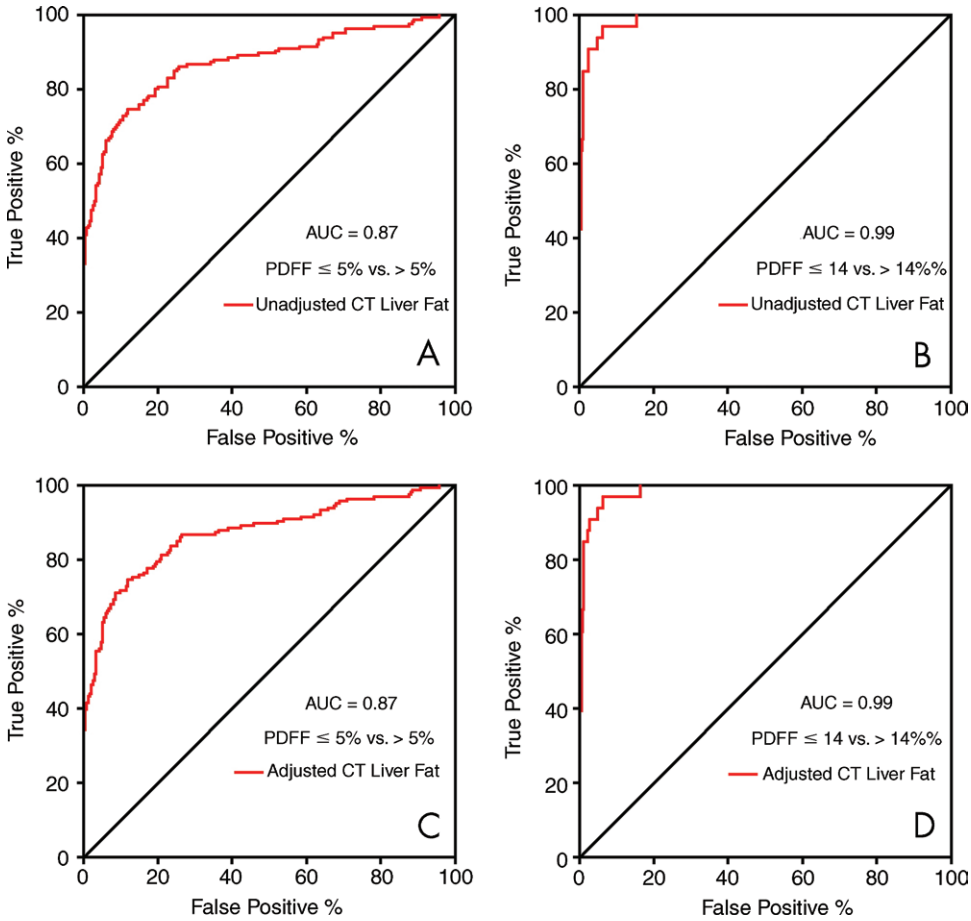

Figure 4: Receiver operating characteristic curves plotted as the percentage of true-positive results (sensitivity) against the percentage of false-positive results (100% specificity). *A*, Unadjusted quantitative CT liver fat measurements to correctly classify study participants with proton density fat fraction (PDFF) greater than 5% (mild steatosis threshold). *B*, Unadjusted quantitative CT liver fat measurements to correctly classify study participants with PDFF greater than 14% (moderate steatosis threshold). *C*, Adjusted quantitative CT liver fat measurements to correctly classify study participants with PDFF greater than 5%. *D*, Adjusted quantitative CT liver fat measurements to correctly classify study participants with PDFF greater than 14%. AUC = area under the receiver operating characteristic curve.

In the past, most studies (26–30) with CT classified liver fat content as normal, mild, moderate, or severe steatosis on the basis of liver Hounsfield units, liver-spleen Hounsfield unit difference, or liver-to-spleen Hounsfield unit ratio. However, this grading system is semiquantitative and lacks precision. Recently, several studies (23,31) have quantified liver fat content by using a formula calculated from unenhanced liver Hounsfield units on the basis of a linear correlation with MRI PDFF. However, these studies used CT scanners from one manufacturer and the bias between scanners from different vendors has not been identified. Quantitative CT measures liver fat on a continuous percentage scale consistent with MRI-derived PDFF, and the calibration phantom could eliminate deviations caused by differences between CT scanners (32,33). Our study showed that compared with quantitative CT, measurement of liver Hounsfield units without the calibration phantom had a similar correlation with CSE MRI PDFF. The correlations of liver-spleen Hounsfield unit difference and liver-to-spleen Hounsfield unit ratio with MRI PDFF were poorer, showing that the inclusion of spleen Hounsfield units in the assessment of liver fat introduces additional errors.

Iron deposition in the liver exacerbates the T2* effect because of its magnetic susceptibility, and R2* is directly proportional to the liver iron content (21,34). The R2* value did not exceed the normal range in any of the 400 participants, and the effect of liver iron on the CT fat measurement is estimated to be less than 1%. In addition, the mDixon Quant sequence has an internal T2* correction and the impact of iron deposition on MRI PDFF was negligible (35).

In clinical practice, the frequent use of CT examinations covering the liver makes these examinations available for liver fat quantification, adding value to them without additional radiation. Therefore, quantitative CT liver fat measurement may present a valuable opportunity for screening and diagnosis of nonalcoholic fatty liver disease.

We acknowledge that our study had limitations. Our participants were healthy and the number of participants with moderate or severe steatosis (liver fat content > 14%) was small (<10%). The highest PDFF measurement was 28%, so the ability of quantitative CT to help evaluate severe steatosis was not analyzed. A single CT protocol was used in our study and the

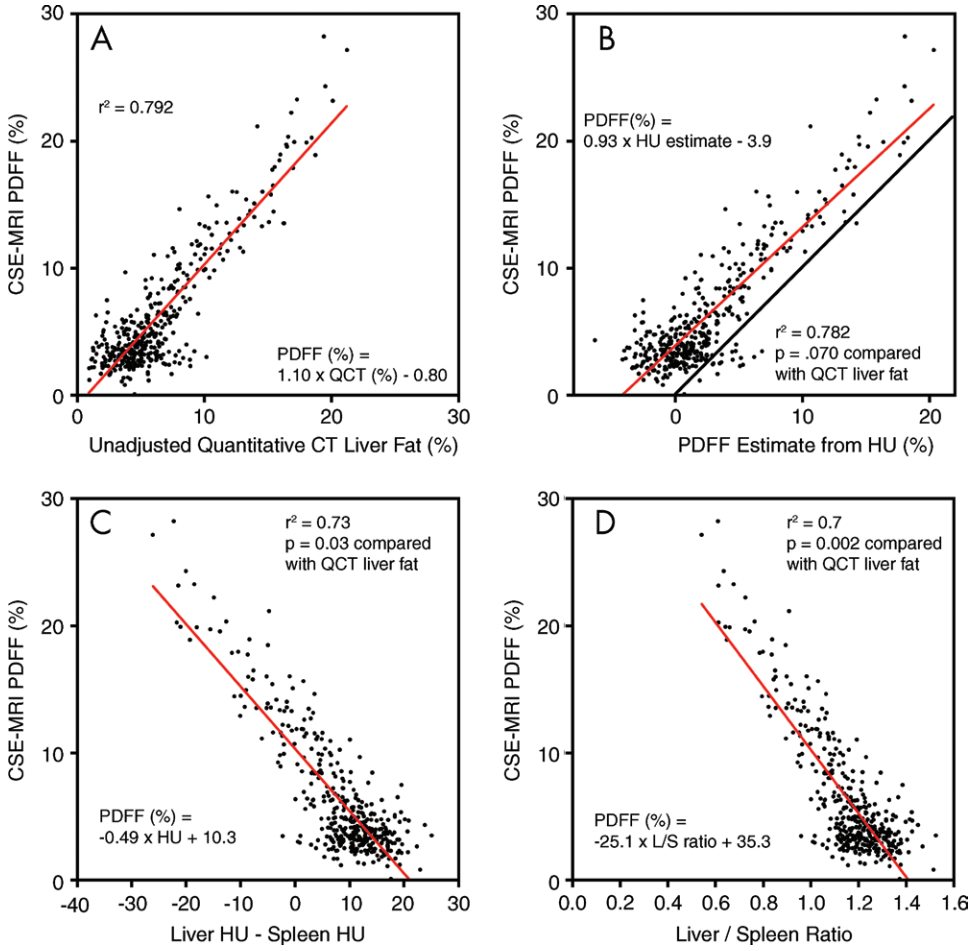

Figure 5: Scatterplots comparing the correlations between chemical shift–encoded (CSE) MRI proton density fat fraction (PDFF) measurements in the liver with, *A*, unadjusted quantitative CT (QCT) measurements in the liver, *B*, PDFF values estimated from Hounsfield unit measurements in the liver by using a published calibration curve (23), *C*, the difference between liver and spleen Hounsfield unit measurements, and, *D*, the ratio of liver-to-spleen (L/S) Hounsfield unit measurements. The *P* values indicate the statistical significance of the difference between the correlation coefficients in *B*, *C*, and *D*, and the correlation coefficient in *A*. The red lines and equations are the linear regression lines. The black line in *B* is the line of identity.

effect of altering CT acquisition and reconstruction parameters, to our knowledge, has not been studied. Furthermore, studies with CT and MRI scanners from different manufacturers are required to guarantee the generalizability of this approach.

In conclusion, as a noninvasive biomarker, quantitative CT liver fat exhibited good correlation with MRI proton density fat fraction measured by mDixon Quant. Therefore, quantitative CT could serve as a reliable screening and quantitative tool for hepatic steatosis.

Author contributions: Guarantors of integrity of entire study, Z.G., G.M.B., X.C.; study concepts/study design or data acquisition or data analysis/interpretation, all authors; manuscript drafting or manuscript revision for important intellectual content, all authors; approval of final version of submitted manuscript, all authors; agrees to ensure any questions related to the work are appropriately resolved, all authors; literature research, Z.G., K.L., Y.Z., J.K.B., P.J.P.; clinical studies, Z.G., K.L., W.L., W.Z., Y.Z., L.X., L.W., X.C.; experimental studies, L.X., J.K.B., X.C.; statistical analysis, Z.G., G.M.B.; and manuscript editing, Z.G., G.M.B., L.X., L.W., J.K.B., X.C., P.J.P.

Disclosures of Conflicts of Interest: Z.G. disclosed no relevant relationships. **G.M.B.** disclosed no relevant relationships. **K.L.** disclosed no relevant relationships. **W.L.** disclosed no relevant relationships. **W.Z.** disclosed no relevant relationships. **Y.Z.** disclosed no relevant relationships. **L.X.** disclosed no relevant relationships. **L.W.** disclosed no relevant relationships. **J.K.B.** Activities related to the present article: disclosed no relevant relationships. Activities not related to the present article: **J.K.B.** Activities related to the present article: disclosed no relevant relationships. Activities not related to the present article: disclosed money paid to author from Mindways for stock and employment. Other relationships: disclosed no relevant relationships. **X.C.** disclosed no relevant relationships. **P.J.P.** Activities related to the present article: disclosed no relevant relationships. Activities not related to the present article: disclosed money paid to author for consultancy from Bracco; disclosed stock/stock options from Shine, Elucent, and Cellectar. Other relationships: disclosed no relevant relationships.

References

1. Chalasani N, Younossi Z, Lavine JE, et al. The diagnosis and management of nonalcoholic fatty liver disease: practice guideline by the American Gastroenterological Association, American Association for the Study of Liver Diseases, and American College of Gastroenterology. Gastroenterology 2012;142(7):1592–1609.
2. Younossi ZM, Koenig AB, Abdelatif D, Fazel Y, Henry L, Wymer M. Global epidemiology of nonalcoholic fatty liver disease-Meta-analytic assessment of prevalence, incidence, and outcomes. Hepatology 2016;64(1):73–84.
3. Wree A, Broderick L, Canbay A, Hoffman HM, Feldstein AE. From NAFLD to NASH to cirrhosis-new insights into disease mechanisms. Nat Rev Gastroenterol Hepatol 2013;10(11):627–636.
4. El-Badry AM, Breitenstein S, Jochum W, et al. Assessment of hepatic steatosis by expert pathologists: the end of a gold standard. Ann Surg 2009;250(5):691–697.

5. Dasarathy S, Dasarathy J, Khiyami A, Joseph R, Lopez R, McCullough AJ. Validity of real time ultrasound in the diagnosis of hepatic steatosis: a prospective study. J Hepatol 2009;51(6):1061–1067.
6. Lee SS, Park SH, Kim HJ, et al. Non-invasive assessment of hepatic steatosis: prospective comparison of the accuracy of imaging examinations. J Hepatol 2010;52(4):579–585.
7. Saadeh S, Younossi ZM, Remer EM, et al. The utility of radiological imaging in nonalcoholic fatty liver disease. Gastroenterology 2002;123(3):745–750.
8. Park SH, Kim PN, Kim KW, et al. Macrovesicular hepatic steatosis in living liver donors: use of CT for quantitative and qualitative assessment. Radiology 2006;239(1):105–112.
9. Pickhardt PJ, Park SH, Hahn L, Lee SG, Bae KT, Yu ES. Specificity of unenhanced CT for non-invasive diagnosis of hepatic steatosis: implications for the investigation of the natural history of incidental steatosis. Eur Radiol 2012;22(5):1075–1082.
10. Cropp RJ, Seslija P, Tso D, Thakur Y. Scanner and kVp dependence of measured CT numbers in the ACR CT phantom. J Appl Clin Med Phys 2013;14(6):4417.
11. Bhat V, Velandai S, Belliappa V, Illayraja J, Halli KG, Gopalakrishnan G. Quantification of Liver Fat with mDIXON Magnetic Resonance Imaging, Comparison with the Computed Tomography and the Biopsy. J Clin Diagn Res 2017;11(7):TC06–TC10.
12. Kühn JP, Hernando D, Muñoz del Rio A, et al. Effect of multipeak spectral modeling of fat for liver iron and fat quantification: correlation of biopsy with MR imaging results. Radiology 2012;265(1):133–142.
13. Tang A, Tan J, Sun M, et al. Nonalcoholic fatty liver disease: MR imaging of liver proton density fat fraction to assess hepatic steatosis. Radiology 2013;267(2):422–431.
14. Yokoo T, Serai SD, Pirasteh A, et al. Linearity, Bias, and Precision of Hepatic Proton Density Fat Fraction Measurements by Using MR Imaging: A Meta-Analysis. Radiology 2018;286(2):486–498.
15. Kang BK, Yu ES, Lee SS, et al. Hepatic fat quantification: a prospective comparison of magnetic resonance spectroscopy and analysis methods for chemical-shift gradient echo magnetic resonance imaging with histologic assessment as the reference standard. Invest Radiol 2012;47(6):368–375.
16. Reeder SB, Hu HH, Sirlin CB. Proton density fat-fraction: a standardized MR-based biomarker of tissue fat concentration. J Magn Reson Imaging 2012;36(5):1011–1014.
17. Engelke K. Quantitative Computed Tomography-Current Status and New Developments. J Clin Densitom 2017;20(3):309–321.
18. Cheng X, Blake GM, Brown JK, et al. The measurement of liver fat from single-energy quantitative computed tomography scans. Quant Imaging Med Surg 2017;7(3):281–291.
19. Xu L, Duanmu Y, Blake GM, et al. Validation of goose liver fat measurement by QCT and CSE-MRI with biochemical extraction and pathology as reference. Eur Radiol 2018;28(5):2003–2012.
20. Bland JM, Altman DG. Statistical methods for assessing agreement between two methods of clinical measurement. Lancet 1986;1(8476):307–310.
21. Kühn JP, Meffert P, Heske C, et al. Prevalence of Fatty Liver Disease and Hepatic Iron Overload in a Northeastern German Population by Using Quantitative MR Imaging. Radiology 2017;284(3):706–716.
22. Cohen J. A Coefficient of Agreement for Nominal Scales. Educ Psychol Meas 1960;20(1):37–46.
23. Pickhardt PJ, Graffy PM, Reeder SB, Hernando D, Li K. Quantification of Liver Fat Content With Unenhanced MDCT: Phantom and Clinical Correlation With MRI Proton Density Fat Fraction. AJR Am J Roentgenol 2018;211(3):W151–W157.
24. Satapathy SK, Sanyal AJ. Epidemiology and Natural History of Nonalcoholic Fatty Liver Disease. Semin Liver Dis 2015;35(3):221–235.
25. Baumeister SE, Völzke H, Marschall P, et al. Impact of fatty liver disease on health care utilization and costs in a general population: a 5-year observation. Gastroenterology 2008;134(1):85–94.
26. Zeb I, Li D, Nasir K, Katz R, Larijani VN, Budoff MJ. Computed tomography scans in the evaluation of fatty liver disease in a population based study: the multi-ethnic study of atherosclerosis. Acad Radiol 2012;19(7):811–818.
27. Kodama Y, Ng CS, Wu TT, et al. Comparison of CT methods for determining the fat content of the liver. AJR Am J Roentgenol 2007;188(5):1307–1312.
28. Schwenzer NF, Springer F, Schraml C, Stefan N, Machann J, Schick F. Non-invasive assessment and quantification of liver steatosis by ultrasound, computed tomography and magnetic resonance. J Hepatol 2009;51(3):433–445.
29. Hahn L, Reeder SB, Muñoz del Rio A, Pickhardt PJ. Longitudinal Changes in Liver Fat Content in Asymptomatic Adults: Hepatic Attenuation on Unenhanced CT as an Imaging Biomarker for Steatosis. AJR Am J Roentgenol 2015;205(6):1167–1172.
30. Zhang Y, Wang C, Duanmu Y, et al. Comparison of CT and magnetic resonance mDIXON-Quant sequence in the diagnosis of mild hepatic steatosis. Br J Radiol 2018;91(1091):20170587.
31. Kramer H, Pickhardt PJ, Kliewer MA, et al. Accuracy of Liver Fat Quantification With Advanced CT, MRI, and Ultrasound Techniques: Prospective Comparison With MR Spectroscopy. AJR Am J Roentgenol 2017;208(1):92–100.
32. Weigert JM. QCT, the most accurate method of measuring bone mineral density? J Bone Miner Res 1997;12(11):1954–1955.
33. Bligh M, Bidaut L, White RA, Murphy WA Jr, Stevens DM, Cody DD. Helical multidetector row quantitative computed tomography (QCT) precision. Acad Radiol 2009;16(2):150–159.
34. Sharma P, Altbach M, Galons JP, Kalb B, Martin DR. Measurement of liver fat fraction and iron with MRI and MR spectroscopy techniques. Diagn Interv Radiol 2014;20(1):17–26.
35. Kukuk GM, Hittatiya K, Sprinkart AM, et al. Comparison between modified Dixon MRI techniques, MR spectroscopic relaxometry, and different histologic quantification methods in the assessment of hepatic steatosis. Eur Radiol 2015;25(10):2869–2879.